Wrap reduction algorithm for Fringe Projection Profilometry

Miguel Arevalillo-Herráez[a,*], Jaume Segura-García[a], Pablo Arnau-González[a], Stamos Katsigiannis[b]

[a]*Departament d'Informàtica, Universitat de València, Spain*
[b]*Department of Computer Science, Durham University, UK*

Abstract

Carrier removal has been typically associated with wrap reduction, and its application has strongly been recommended as a previous step to phase unwrapping. In general, the carrier signal contributes to an increase of the number of wraps, and its removal leads to a reduction of the number of phase inconsistencies, having a positive impact on the subsequent unwrapping operation. In this paper, we show that phase wrap reduction can be better tackled by other alternative and more effective methods that exploit local information and attempt to also remove the signal component associated with the object's surface. The results are analyzed on a series of real fringe patterns and confirm the better performance of the proposed method, which leads to signals with a lesser number of wraps than by just removing the carrier.

Keywords: wrap reduction, carrier removal, phase unwrapping

1. Introduction

In Fringe Projection Profilometry (FPP), a sinusoidal fringe pattern is projected onto an object surface, giving as a result a deformed pattern that is captured with a camera. The grabbed image can then be processed to recover a phase signal, whose value is related to the height of the surface at each point. This is done by choosing one out of a variety of well-established phase retrieval methods [1, 2], such as Fourier [3], wavelet [4], FIR Hilbert transformers [5], Shearlet transforms [6] or phase shifting techniques [7].

In general, and because of the angular nature of phase values and the carrier related phase component introduced by the projected fringe pattern, all these methods recover a signal

$$\phi_w(x,y) = \mathcal{W}\left[2\pi f(x,y) + \phi_h(x,y)\right], \tag{1}$$

where $\phi_h(x,y)$ is the phase component related to the surface height at position (x,y); $f(x,y)$ is the carrier related term; and $\mathcal{W}$ denotes the wrapping operator, which returns an angle to its principal argument.

The retrieved signal $\phi_w(x,y)$ is hence bounded in the range $(-\pi,\pi]$, and discontinuities (wraps) that are due to the use of principal arguments and should not be present on the unbounded height measurements appear on the result. The recovery of the surface height from $\phi_w(x,y)$ requires the cancellation of both the effect of the wrapping operator $\mathcal{W}$ and the carrier related component $2\pi f(x,y)$.

The first of these operations is achieved by using an unwrapping algorithm. The second one, by using a carrier removal technique. Multiple unwrapping algorithms do exist, as a consequence of a vast research on this area. They are generally classified into global error minimization algorithms [8, 9, 10], branch-cut methods [11, 12], quality guided techniques [13, 14], region-growing approaches [15, 16], deep learning methods [17, 18] and hybrid approaches [19, 20]. Carrier removal has also been widely studied, including methods that operate in the Fourier [21, 22, 23, 24] and spatial domains [25, 24, 26].

The carrier removal operation can take place before or after unwrapping. However, the carrier frequency translates into a monotonically increasing (or decreasing) component in the phase function, which makes it grow faster and hence increases the number of wraps [24] and the complexity of phase unwrapping [24, 25, 27]. Therefore, it is highly recommended to use carrier removal as a wrap reduction algorithm before unwrapping. This has led to a confusion between the terms "carrier removal" and "wrap reduction", which have been used interchangeably in the literature. In fact, techniques announced as wrap reduction methods [28, 29, 30, 23, 24, 31] restrict themselves to approximate and remove a linear phase component from the signal, and share the same computational procedures as for eliminating the carrier. However, wrap reduction methods should just focus on subtracting any continuous component that makes the signal easier to unwrap, and shall not restrict to a linear function. This means that local slopes in the object surface could also be subtracted, in order to produce a smoother signal that fits into fewer (or a single) $(-\pi,\pi]$ cycles.

In this paper, we present a phase reduction method that exploits the local information around each phase value to remove a phase component that includes not only the carrier, but also part of the signal related to the surface heights. In this way,

*Corresponding author
Email addresses: miguel.arevalillo@uv.es (Miguel Arevalillo-Herráez), jaume.segura@uv.es (Jaume Segura-García), pablo.arnau@uv.es (Pablo Arnau-González), stamos.katsigiannis@durham.ac.uk (Stamos Katsigiannis)

the method is able to deal with multiple frequencies in local regions, and seamlessly adapts to them to yield a more effective wrap reduction than typical carrier removal techniques.

2. Current wrap reduction methods

Wrap reduction/carrier removal methods aim to cancel the $2\pi f(x, y)$ term from Eq. 1, in order to isolate the phase component related to the object heights $\phi_h(x, y)$. This operation can be either performed in Fourier or spatial domain.

Methods that operate in the frequency spectrum assume a linear carrier, and are specially suitable when Fourier methods are used for phase retrieval. Otherwise, they require the computation of a 2D discrete Fourier transform (DFT). The assumption of a linear carrier turns Eq. 1 into

$$\phi_w(x, y) = \mathcal{W}\left[2\pi f_x x/C + 2\pi f_y y/R + \phi_h(x, y)\right], \qquad (2)$$

where R is the number of rows; C is the number columns; and f_x and f_y are the carrier frequency in the x- and y- direction, respectively.

To isolate the surface-related component, let us consider the complex signal

$$\begin{aligned} \psi(x, y) &= \cos(\phi_w(x, y)) + j\sin(\phi_w(x, y)) \\ &= e^{j\phi_w(x,y)} \\ &= e^{j\left(2\pi f_x x/C + 2\pi f_y y/R + \phi_h(x,y)\right)} \\ &= e^{j2\pi f_x x/C} \cdot e^{j2\pi f_y y/R} \cdot e^{j\phi_h(x,y)} \end{aligned} \qquad (3)$$

and apply the 2-D DFT operator $\mathcal{F}(\cdot)$ to it. In the frequency domain, the first and second terms in the last row of Eq. 3 have a spectra with a single peak located at positions $(f_x, 0)$ and $(0, f_y)$, respectively. Since the product in this equation becomes a convolution in the Fourier domain, the effect of these first two terms in the DFT is a shift (f_x, f_y) of the term $\mathcal{F}(e^{j\phi_h(x,y)})$. Undoing this shift and applying an inverse Fourier transform yields the term $e^{j\phi_h(x,y)}$, and the wrapped phase of the signal $\phi_h(x, y)$ can then be obtained as the complex argument of the result.

The accuracy of frequency-based methods depends on the estimate of the shift (f_x, f_y). Initially, methods were restricted to integer values [21, 32]. In this case, carrier removal can be computed by using Algorithm 1, where $\mathcal{R}(\cdot)$ and $\mathcal{I}(\cdot)$ stand for the real and imaginary parts of a complex number, respectively. However, frequency-based methods have been recently extended to support rational displacements by using zero padding [22, 33], iterative methods [23, 30], or more accurate estimations of the 2-D fundamental frequency [31]. In these cases, and once the shift has been estimated, carrier removal is directly performed in the spatial domain as

$$\phi'_w(x, y) = \mathcal{W}\left[\phi_w(x, y) - 2\pi f_x x/C - 2\pi f_y y/R\right] \qquad (4)$$

With regard to methods that fully operate in the spatial domain, some are also based on the assumption of a linear carrier

(1) build $\psi(x, y) = e^{j\phi_w(x,y)} = \cos(\phi_w(x, y)) + j\sin(\phi_w(x, y))$
(2) compute $\Psi(u, v) = \mathcal{F}\{\psi(x, y)\}$
(3) compute $f_x, f_y = \arg\max_{u,v} |\Psi(u, v)|$
(4) compute $\Psi'(u, v) = \Psi(u + f_x, v + f_y)$
(5) compute $\psi'(x, y) = \mathcal{F}^{-1}\{\Psi'(u, v)\}$
(6) compute
$\phi'_w(x, y) = \arg(\psi'(x, y)) = \arctan 2(\mathcal{I}(\psi'(x, y))/\mathcal{R}(\psi'(x, y)))$

Algorithm 1: Pseudo-code for the wrap reduction algorithm in the Fourier Domain [28].

signal, and attempt to estimate the slopes m_x and m_y in the x- and y- directions by using the average [25] or mode [24] of the first derivative values in each axis. These values are then used instead of the frequencies f_x and f_y, turning Eq. 4 into

$$\phi'_w(x, y) = \mathcal{W}\left[\phi_w(x, y) - m_x x - m_y y\right] \qquad (5)$$

Some other methods support the removal of non linear carriers, which are approximated by using series expansion [34] or Zernike polynomials [26]. The carrier component can also be eliminated by subtracting a reference phase signal computed from the projection of the fringe pattern on a flat surface [3], but this method requires the acquisition of a second independent image.

In any case, a total removal of the wraps is by no means guaranteed, because the signal $\phi_h(x, y)$ may still expand across several $(-\pi, \pi]$ cycles after carrier removal. Still, the wrap reduction achieved by carrier cancellation usually contributes to simplifying the subsequent unwrapping operation.

3. Proposed method

The carrier frequency usually corresponds to the fundamental frequency of the signal in Eq. 3, and this translates into an added slope in the wrapped phase signal $\phi_w(x, y)$. Although removing the carrier-related component of the signal usually makes the signal fit in fewer $(-\pi, \pi]$ cycles, we can achieve a greater reduction by subtracting a shape that also contains a part of the surface-related component of the signal.

In essence, carrier removal attempts to separate the original wrapped signal $\phi_w(x, y)$ into two components that add up to the original signal after the application of the wrapping operator $\mathcal{W}$. The first component is the carrier, $\phi_c(x, y) = m_x x + m_y y$. This is generally linear and takes the shape of a ramp with constant slopes m_x and m_y along the x- and y- axes, respectively. The second, component corresponds to the remainder of the signal $\phi'_w(x, y) = \mathcal{W}(\phi_w(x, y) - \phi_c(x, y))$. If $\mathcal{U}$ represents the unwrapping operator, the unwrapped signal $\phi(x, y) = \mathcal{U}(\phi_w(x, y))$ can then obtained as $\mathcal{U}(\phi'_w(x, y)) + \phi_c(x, y)$, or directly by $\mathcal{U}(\phi'_w(x, y))$ if only the surface-related component is desired. Since the signal $\phi'_w(x, y)$ usually has less wraps than the original signal $\phi_w(x, y)$, the unwrapping problem is generally simplified. The ideal case is when carrier subtraction results in a signal $\phi'_w(x, y)$ which does not require unwrapping, as then the unwrapped surface-related component of the signal $\phi(x, y)$ can be obtained directly as $\phi'_w(x, y)$. Fig. 1 shows a schematic

diagram that describes the application of carrier removal to the phase unwrapping problem, according to the explanation above.

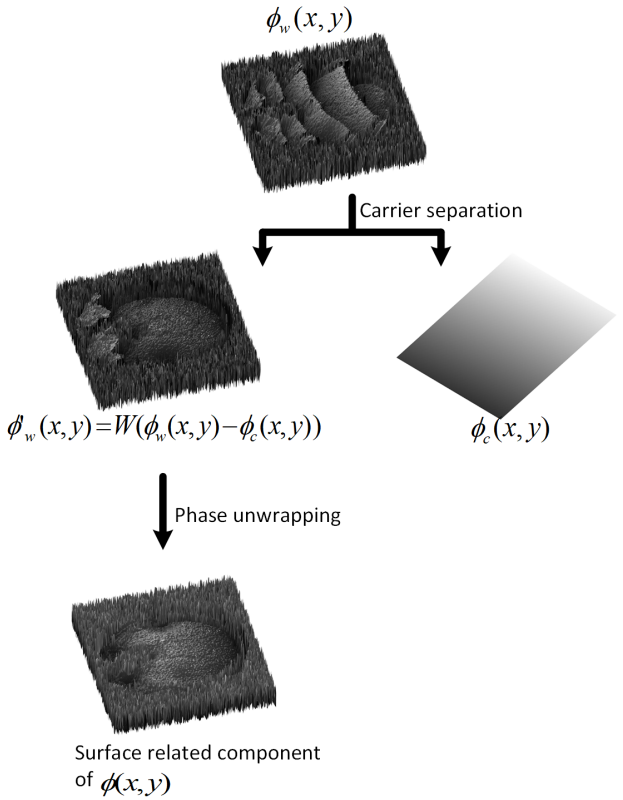

Figure 1: Step-by-step illustration of the carrier removal process.

Maintaining the same signal separation strategy, we eliminate the ramp-shaped restriction from the first phase map $\phi_c(x, y)$. Instead, we allow for more flexible shapes that help further reducing the number of wraps in the second signal component $\phi'_w(x, y)$. One basic requirement is that the $\phi_c(x, y)$ is smooth and does not contain any discontinuities, as otherwise they would be directly transferred into the final result. One possible way to generate this surface is by locally deciding the slopes in the x- and y- axis at each pixel, as a function of the wrapped first differences in each direction for the surrounding rows and columns; and then integrating the slopes to build the subtracted signal. To compute these local slopes, we use the average slope method [25]. However, we compute it independently for each row/column, rather than estimating a single slope for the whole image.

The neighbourhood considered for the computation of the slopes has a band shape, in both the horizontal an vertical axis. The width of this band is determined by w, which is the only parameter for the algorithm. When $w = 0$, only first differences between phase values in the the same row/column and the ones in the previous are considered, as it is shown in Figure 2(a).

More specifically, the local slopes are estimated as

$$\Delta_x(\cdot, y) = \begin{cases} 0, & \text{if } y = 1 \\ \frac{1}{R}\sum_{i=1}^{R} \mathcal{W}\left[\phi_w(i, y) - \phi_w(i, y-1)\right], & \text{otherwise} \end{cases} \quad (6)$$

$$\Delta_y(x, \cdot) = \begin{cases} 0, & \text{if } x = 1 \\ \frac{1}{C}\sum_{i=1}^{C} \mathcal{W}\left[\phi_w(x, i) - \phi_w(x-1, i)\right], & \text{otherwise} \end{cases} \quad (7)$$

where $\Delta_x(\cdot, y)$ is the estimated slope in the x-direction for any pixel located at column y; and $\Delta_y(x, \cdot)$ is the estimated slope in the y-direction for any pixel located at row x.

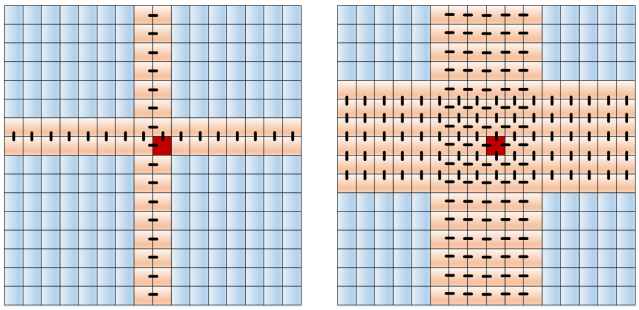

Figure 2: phase values considered on a 16 x 16 signal to compute $\Delta_x(x, y)$ and $\Delta_y(x, y)$ at the pixel marked in red close to the center of the image, when $w = 0$ (a); and when $W = 2$ (b)

Once $\Delta_x(\cdot, y)$ and $\Delta_y(x, \cdot)$ have been computed, the surface to subtract can be obtained by integrating the first differences as

$$\phi_c(x, y) = \sum_{i=2}^{y} \Delta_x(\cdot, i) + \sum_{i=2}^{x} \Delta_y(i, \cdot) \quad (8)$$

and the remaining signal to be unwrapped would be:

$$\phi'_w(x, y) = \mathcal{W}\left[\phi_w(x, y) - \phi_c(x, y)\right] \quad (9)$$

The signal $\phi_c(x, y)$ will be added back to the result of unwrapping $\phi'_w(x, y)$, to produce the final unwrapped result $\phi(x, y)$; and the surface-related component can be recovered by carrier subtraction on $\phi(x, y)$.

The fact that $\Delta_x(\cdot, y)$ and $\Delta_y(x, \cdot)$ take the same value for all pixels in the same column and row, respectively, guarantees a path independent integration from the first differences in $\phi_c(x, y)$. This can be easily understood from Fig. 3, which shows a 2 x 2 grid, along with the phase differences between the values in the grid. As it can be observed, the addition of the first differences along any 2 x 2 closed path always yields a zero value.

The computation of the slopes $\Delta_x(\cdot, y)$ and $\Delta_y(x, \cdot)$ in Eqs. 6 and 7 can be easily generalized to larger values of the parameter w, whose effect is to enlarge the band-shaped regions that are considered in the calculation. Figure 2(b) shows an example for $w = 2$. For pixels at a distance $> w$ from the borders of the image, the width of the band is $2(w + 1)$ and the number

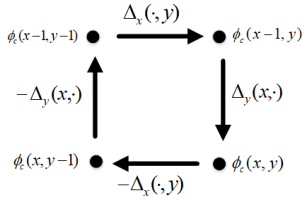

Figure 3: 2 x 2 pixel grid in signal $\phi_c(x, y)$

of second differences considered for $\Delta_x(\cdot, y)$ is $(2w + 1)C$, and $(2w+1)R$ for $\Delta_y(x, \cdot)$. For pixels closer to the border, the part of the band that falls outside the image is simply discarded from the computation, and Eqs. 6 and 7 turn into

$$\Delta_x(\cdot, y) = \frac{\sum_{i=1}^{R} \sum_{j=f_y}^{l_y} \mathcal{W}\left[\phi(i, j) - \phi(i, j-1)\right]}{(l_y - f_y + 1)R} \tag{10}$$

$$\Delta_y(x, \cdot) = \frac{\sum_{i=f_x}^{l_x} \sum_{j=1}^{C} \mathcal{W}\left[\phi(i, j) - \phi(i-1, j)\right]}{(l_x - f_x + 1)C} \tag{11}$$

where $f_x = \max(1, x - w)$ and $l_x = \min(C, x + w)$ are the first and last columns whose first differences are considered; and $f_y = \max(1, y - w)$ and $l_y = \min(R, y + w)$ are the first and last rows whose first differences are taken into account.

The larger the value of w, the smoother the surface will be. A wider band limits the changes between the gradients $\Delta_x(i, \cdot)$ and $\Delta_x(i + 1, \cdot)$; and between $\Delta_y(\cdot, j)$ and $\Delta_y(\cdot, j + 1)$, which are the second differences of the signal in each direction. This is because their computation differs in just one row/column, and the rest are shared between both calculations. This yields a theoretical maximum change between two consecutive values of $\Delta_x(x, \cdot)$ or $\Delta_y(\cdot, y)$ of $2\pi/(2w + 1)$.

Fig. 4 summarizes the computation of the signal separation described in this section, and Fig. 5 illustrates the practical application of the proposed method. The local slope estimates generally result in a higher reduction the number of wraps, as compared to the global estimate in the carrier removal method. On the negative side, carrier removal does not typically cause a global overhead on the processing pipeline, as it is a necessary step to recover the surface-related component of $\phi(x, y)$ and no significant saving or overhead is caused by running it before or after phase unwrapping. On the contrary, signal separation in the proposed method is an added step that increases the running time of the processing pipeline.

4. Implementation

An efficient implementation of the algorithm can be achieved by first computing the average first wrap differences in the x- direction for each column, $d_x[c], c = 1 \ldots C$; and the average first differences in the y- direction for each row, $d\_y[r], r = 1 \ldots R$. These are computed according to Eqs. 12 and 13 as

$$d_x[c] = \begin{cases} 0, & \text{if } c = 1 \\ \frac{1}{R} \sum_{i=1}^{R} \mathcal{W}\left[\phi_w(i, c) - \phi_w(i, c-1)\right], & \text{otherwise} \end{cases} \tag{12}$$

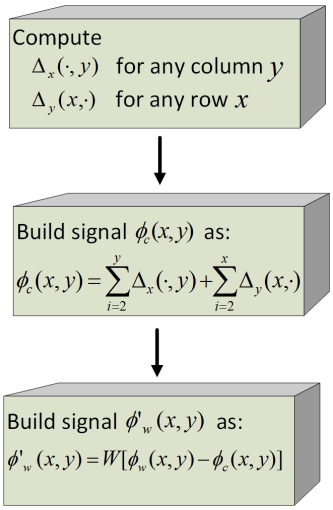

Figure 4: Algorithm to produce the proposed signal separation.

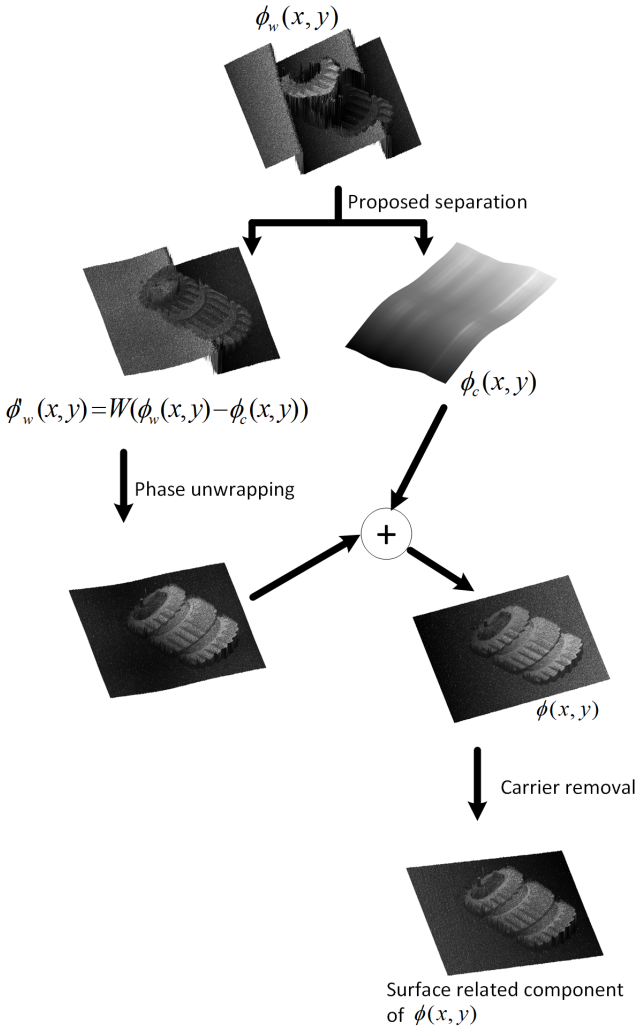

Figure 5: Step-by-step illustration of the proposed method.

$$d_y[r] = \begin{cases} 0, & \text{if } x = 1 \\ \frac{1}{C}\sum_{i=1}^{C} \mathcal{W}\left[\phi_w(r,i) - \phi_w(r-1,i)\right], & \text{otherwise} \end{cases} \quad (13)$$

Then, the averaged values for the band are computed from the values of d_x and d_y

$$\overline{d}_x[c] = \frac{\sum_{i=f_c}^{f_r} d_x[i]}{(l_c - f_c + 1)} \quad (14)$$

$$\overline{d}_y[r] = \frac{\sum_{i=f_r}^{l_r} d_y[i]}{(l_r - f_r + 1)} \quad (15)$$

where $f_c = \max(1, c-w)$ and $l_c = \min(C, c+w)$ are the first and last columns in the band considered; and $f_r = \max(1, r-w)$ and $l_r = \min(R, r+w)$ are the first and last rows. This operation can be sped up for large values of w by computing $\overline{d}_x[c]$ and $\overline{d}_y[r]$ from the previously computed values $\overline{d}_x[c-1]$ and $\overline{d}_y[r-1]$. When $w = 1$, $\overline{d}_x[c] = d_x[c]$, and $\overline{d}_y[r] = d_y[r]$.

After, the average first differences in $\overline{d_x}$ and $\overline{d_y}$ are integrated to yield the vectors $\widehat{d_x}$ and $\widehat{d_y}$. This is done by setting $\widehat{d_x}[1] = \overline{d_x}[1]$ and $\widehat{d_y}[1] = \overline{d_y}[1]$; and iteratively applying the equations:

$$\widehat{d_x}[c] = \widehat{d_x}[c-1] + \overline{d}_x[c] \quad (16)$$

$$\widehat{d_y}[r] = \widehat{d_y}[r-1] + \overline{d}_y[r], \quad (17)$$

starting at indexes $c = 2$ and $r = 2$ and finishing at $c = C$ and $r = R$.

Next, the row vector d_x needs to be replicated R times across the y-axis to build a matrix M_x of size $R \times C$; and the column vector d_y is repeated across the x-axis to build another matrix M_y, also of size $R \times C$. The sum of these two matrices yields the signal $\phi_c(x, y)$, containing the surface to be subtracted. This surface plays the role of the carrier in typical fringe reduction methods based on carrier removal. Finally, the remaining signal component $\phi'_w(x, y)$ to be unwrapped is obtained by using Eq. 9.

5. Results

The efficacy of the proposed carrier removal method has been tested on a variety of phase signals of size 515×512, most of them from FPP. These signals have been used to compare the wrap reduction results with two representative methods. The first one is the classical average slope algorithm [25], that operates in the spatial domain by subtracting the average wrapped phase difference in each direction and has been widely used because of its simplicity and reasonable performance. The second technique operates in the frequency domain and it is based on an accurate estimate of the fundamental frequency of a 2D complex signal built from the phase ϕ_w [31], using the 2D frequency estimation method presented in [35]. To allow for a fair comparison and to ease the visual inspection of the results, a convenient constant has been added to all outputs. This constant minimizes the total number of differences greater than π between adjacent pixels across the entire signal, in an attempt to make the resulting phase fit in a single 2π cycle. In all cases,

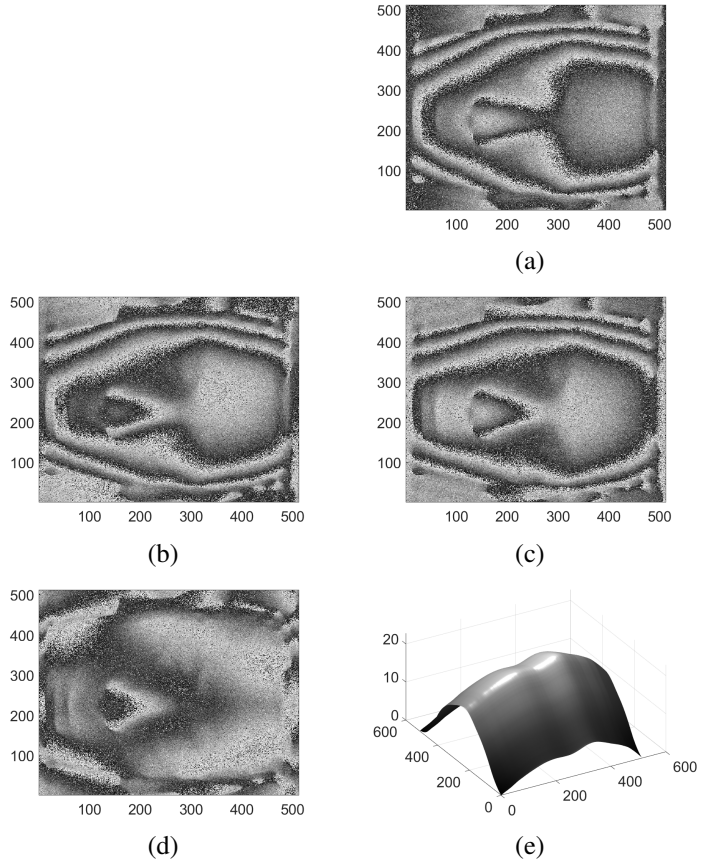

Figure 6: Comparative analysis of algorithms in a noisy wrapped signal that corresponds to a surface measurement on a human face. (a) original wrapped signal obtained by the FFT method [3], including an integer phase shift in the frequency domain; remaining signal component $\phi'_w(x, y)$ after (b) application of carrier removal by the the average slope method [25]; (c) alternative FFT-based wrap reduction method presented in [31]; and (d) the proposed approach. The difference between the signals subtracted in (b) and (d) is illustrated in (e).

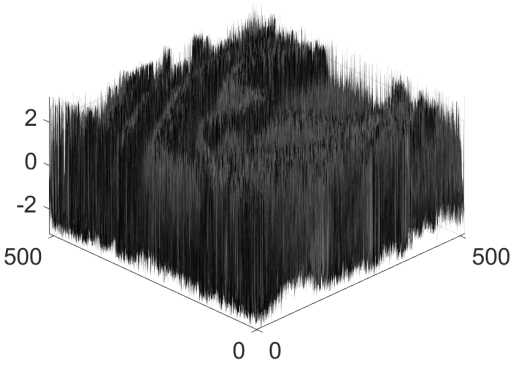

Figure 7: A 3D representation of the signal in Fig. 6(a)

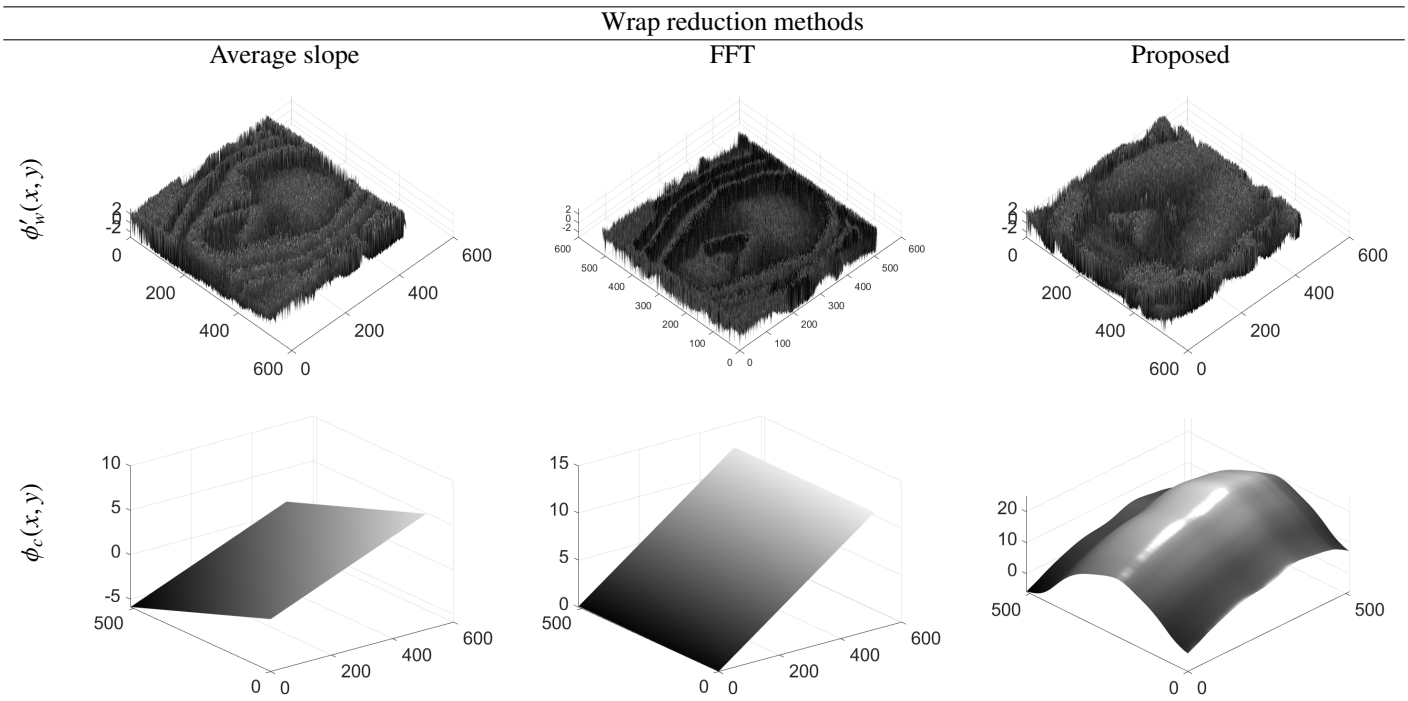

Figure 8: Decomposition of $\phi_w(x,y)$ into signals $\phi'_w(x,y)$ and $\phi_c(x,y)$, in all compared methods

we have set the smoothness parameter w for the proposed algorithm to 32, which has experimentally demonstrated a good trade-off between smoothness and wrap reduction for signals of size 512×512.

The first signal corresponds to a noisy height measurement of a human face (Fig. 6(a)), processed by the FFT method [3]. As in most images used in this section, a range image representation is used, using grey levels to denote phase values from $-\pi$ (black) to π (white). Fig. 7 provides a 3D representation of the signal, which helps the observation of inherently present noise. In this case, the application of phase shifting in the Fourier domain already eliminated some of the wraps caused by the carrier signal, but its performance was limited by the integer shift. The wrap reduction obtained by using the average slope and Fourier methods is shown in Figs. 6(b) and 6(c). Both results are very similar and, although a displacement of the fringes can be observed, the algorithms have not been able to reduce the number of wraps in the original phase map shown in Fig. 6(a). The result for the proposed method is shown in Fig. 6(d). In contrast to the other competing methods, most wraps have been eliminated. Fig. 6(e) shows the difference between the signals subtracted in Figs. 6(b) and 6(d). While a plane with a low slope was subtracted in the former case, the phase component subtracted in the latter case has an adaptive shape that resembles the original signal, and its effect on the number of wraps is clearly more noticeable. Figure 8 focuses on the decomposition of the original wrapped signal, and attempts to emphasize the difference between the signals $\phi_c(x,y)$ obtained by the three competing methods. As it can be observed, both the FFT and average slope methods restrict the shape of $\phi_c(x,y)$ to a linear ramp. On the contrary, the proposed method results in a more elaborate decomposition, in which the signal $\phi_c(x,y)$ combines the carrier with some surface-related component, which helps reducing the remaining wraps in $\phi'_w(x,y)$.

The same comparative analysis was performed on several other signals. The one shown in Fig. 9(a) corresponds to a different human face and was also obtained by using the same method as in the previous case. Again, both the average slope and the FFT-based methods do not yield a significant reduction of the number of wraps, as it can be observed in Figs. 9(b) and 9(c). On the contrary, the proposed method was able to significantly reduce the number of wraps in the original signal. This was again due to the subtraction of a more convenient shape.

The wrapped phase signal in Fig. 10(a) corresponds to the measurement of a human mannequin torso, with part of the head at the right-hand side of the image and an unreliable measurement caused by the a shadow at the left-hand side. In this case, no carrier removal method was applied, causing a number of fringes that extend across the x-axis of the image. Both the FFT and average slope methods achieve a reduction of the wraps. However, only the proposed approach is capable of removing all wraps from the surface of interest, making the unwrapping operation unnecessary. Again, this effect is caused by the subtraction of a phase component whose low frequencies are related to those in the original signal, helping again in achieving a more noticeable effect.

The signal in Fig. 11(a) was obtained by measuring a porcelain figure of a fairy. In this case, we can see that the effect of the FFT method is an effective carrier removal. This method fully eliminates the wraps in the background of the image, but

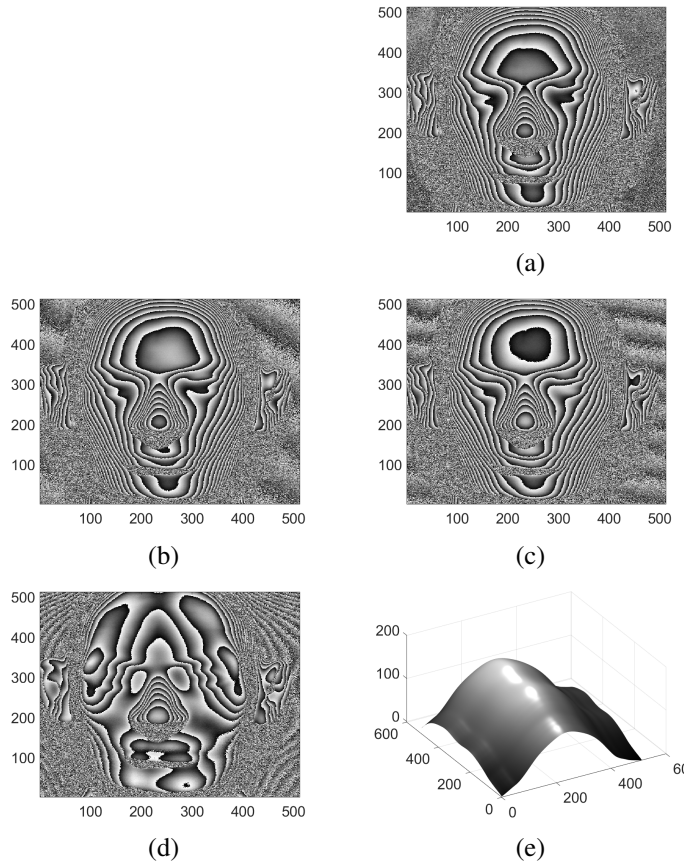

Figure 9: Comparative analysis of algorithms in a wrapped signal that corresponds to a surface measurement on a second human face. (a) original wrapped signal obtained by the FFT method [3], including an integer phase shift in the frequency domain; remaining signal component after (b) application of carrier removal by the the average slope method [25]; (c) alternative FFT-based wrap reduction method presented in [31]; and (d) the proposed approach. The difference between the signals subtracted in (b) and (d) is illustrated in (e).

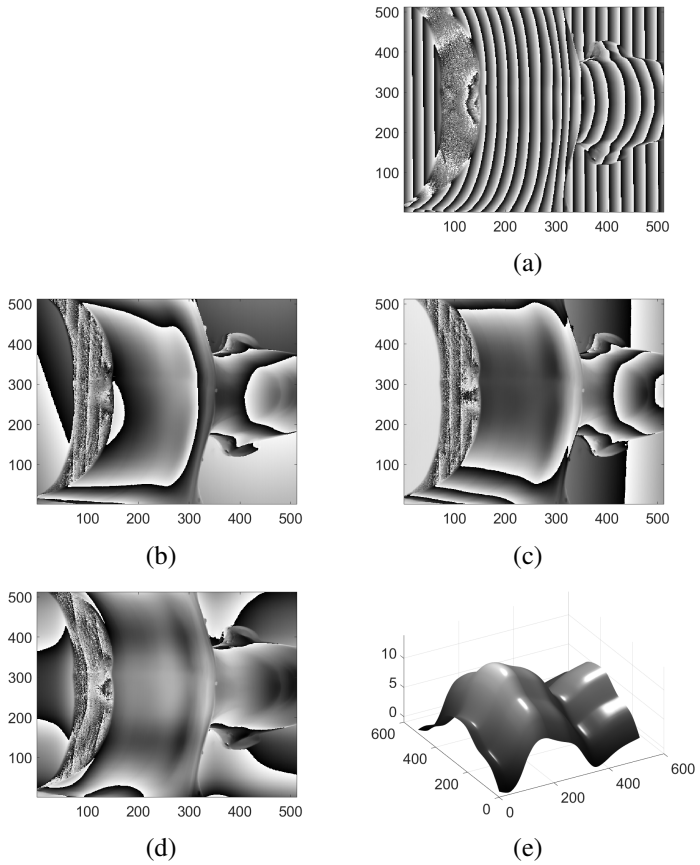

Figure 10: Comparative analysis of algorithms in a wrapped signal that corresponds to a surface measurement on a human mannequin torso, including part of the head. (a) original wrapped signal obtained by the FFT method [3], including an integer phase shift in the frequency domain; remaining signal component after (b) application of carrier removal by the the average slope method [25]; (c) alternative FFT-based wrap reduction method presented in [31]; and (d) the proposed approach. The difference between the signals subtracted in (b) and (d) is illustrated in (e).

leaves a few inside the figure. The average slope method leaves some wraps in the background, but achieves a better effect on the more relevant regions associated with the fairy figure. Our proposed method behaves the best and removes most wraps from the fairy figure, despite that it leaves some wraps in the background. When a background is present, the differences in behaviour between typical carrier removal methods and the proposed technique are specially noticeable. Carrier removal techniques tend to produce a wrap-free background, while the proposed method focuses wrap reduction on the object's surface. The behaviour of the proposed technique is hence preferred when the background location is known and the signal can be masked to unwrap the area of interest only. When this is not the case, the FFT or average slope methods can be seamlessly used to detect areas of constant value and produce such mask.

Another example that clearly shows the benefits of the proposed method on a measurement of an upper body mannequin is shown in Fig. 13(a). As in the previous case, the FFT method works perfect at removing the effect of the carrier frequency, but leaves some wraps in the mannequin. Again, the average slope is more efficient at removing wraps in the most relevant part of the image, but leaves wraps in both the mannequin and the background. On the contrary, the propose techniques removes most wraps from the mannequin.

The last two examples clearly show that the carrier removal and wrap reduction objectives are not necessarily equivalent. In fact, the FFT-based method is clearly superior at the first task. This is generally the case when the carrier is linear and a large part of the signal corresponds to the background. Under such circumstances, the fundamental frequency of the signal $\psi(x, y)$ in Eq. 3 is associated with the carrier, and the FFT-based method is able to accurately estimate it. However, the proposed method behaves considerably better at wrap reduction, achieving a greater and more convenient effect on the areas of interest. The more flexible shape of the signal component subtracted, driven by a more local estimation of the slopes in each region, yields a more intense decrease in the number of wraps.

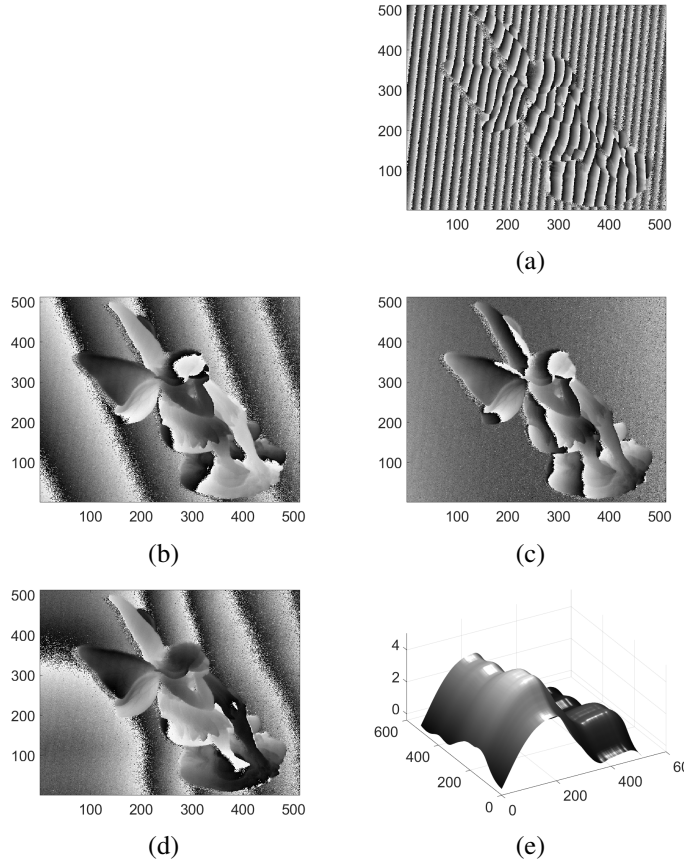

Figure 11: Comparative analysis of algorithms in a wrapped signal that corresponds to the measurement of a porcelain figure of a fairy. (a) original wrapped signal obtained by the FFT method [3], including an integer phase shift in the frequency domain; remaining signal component signal after (b) application of carrier removal by the the average slope method [25]; (c) alternative FFT-based wrap reduction method presented in [31]; and (d) the proposed approach. The difference between the signals subtracted in (b) and (d) is illustrated in (e).

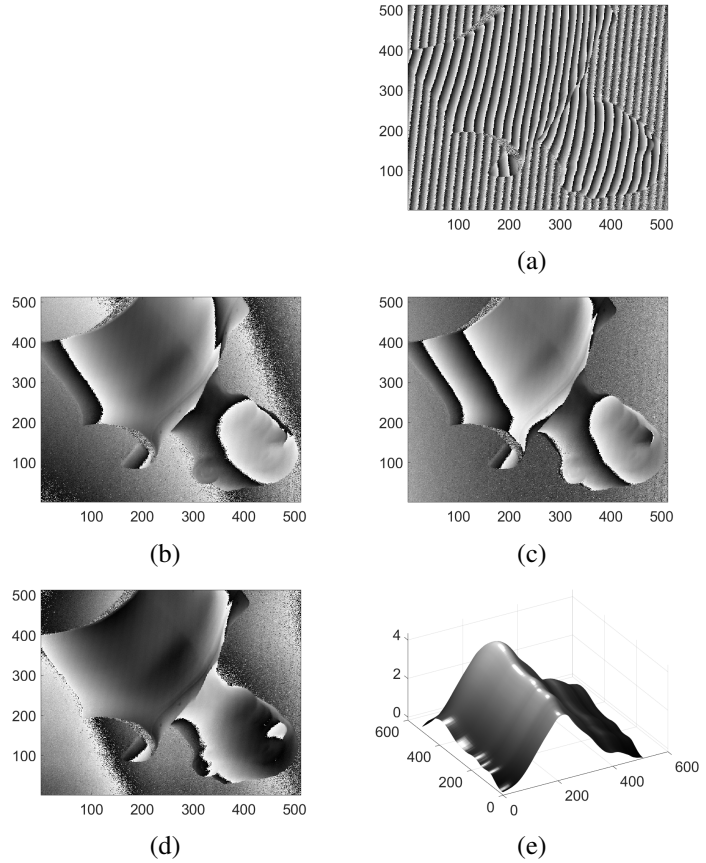

Figure 12: Comparative analysis of algorithms in a wrapped signal that corresponds to the measurement of the upper body mannequin. (a) original wrapped signal obtained by the FFT method [3], including an integer phase shift in the frequency domain; remaining signal component signal after (b) application of carrier removal by the the average slope method [25]; (c) alternative FFT-based wrap reduction method presented in [31]; and (d) the proposed approach. The difference between the signals subtracted in (b) and (d) is illustrated in (e).

6. Conclusions

Despite fundamental differences between the carrier removal and the phase wrap reduction tasks, both terms have been indistinctly used in the literature. Although carrier removal methods generally achieve a wrap reduction on 2-D phase signals, a better effect can be achieved by subtracting an adaptive signal computed from seamlessly estimated local slopes. In this paper, we have proposed an algorithm based on this principle, and showed that such an approach improves the performance of typical carrier removal methods at the specific task of reducing the number of wraps.

Acknowledgment

This research has been supported by project PGC2018-096463-B-I00, funded by MCIN/AEI/10.13039/501100011033 and FEDER Una manera de hacer Europa; project AICO/2021/019, funded by Valencian Regional Government (Spain); and grant Margarita Salas, funded by the Spanish Ministry of Universities.

References

[1] Z. Zhang, Z. Jing, Z. Wang, D. Kuang, Comparison of Fourier transform, windowed Fourier transform, and wavelet transform methods for phase calculation at discontinuities in fringe projection profilometry, Optics and Lasers in Engineering 50 (8) (2012) 1152–1160. doi:10.1016/j.optlaseng.2012.03.004.

[2] C. Quan, W. Chen, C. J. Tay, Phase-retrieval techniques in fringe-projection profilometry, Optics and Lasers in Engineering 48 (2) (2010) 235–243. doi:10.1016/j.optlaseng.2009.06.013.

[3] M. Takeda, H. Ina, S. Kobayashi, Fourier-transform method of fringe-pattern analysis for computer-based topography and interferometry, JOSA 72 (1) (1982) 156–160, publisher: Optical Society of America. doi:10.1364/JOSA.72.000156.

[4] J. Zhong, J. Weng, Phase retrieval of optical fringe patterns from the ridge of a wavelet transform, Opt. Lett. 30 (19) (2005) 2560–2562. doi:10.1364/OL.30.002560.

[5] M. Gdeisat, D. Burton, F. Lilley, M. Arevalillo-Herráez, Fast fringe pattern phase demodulation using FIR Hilbert transformers, Optics Communications 359 (2016) 200–206. doi:10.1016/j.optcom.2015.09.084.

[6] B. Li, C. Tang, X. Zhu, Y. Su, W. Xu, Shearlet transform for phase extraction in fringe projection profilometry with edges discontinuity, Optics and Lasers in Engineering 78 (2016) 91–98. doi:https://doi.org/10.1016/j.optlaseng.2015.10.007.

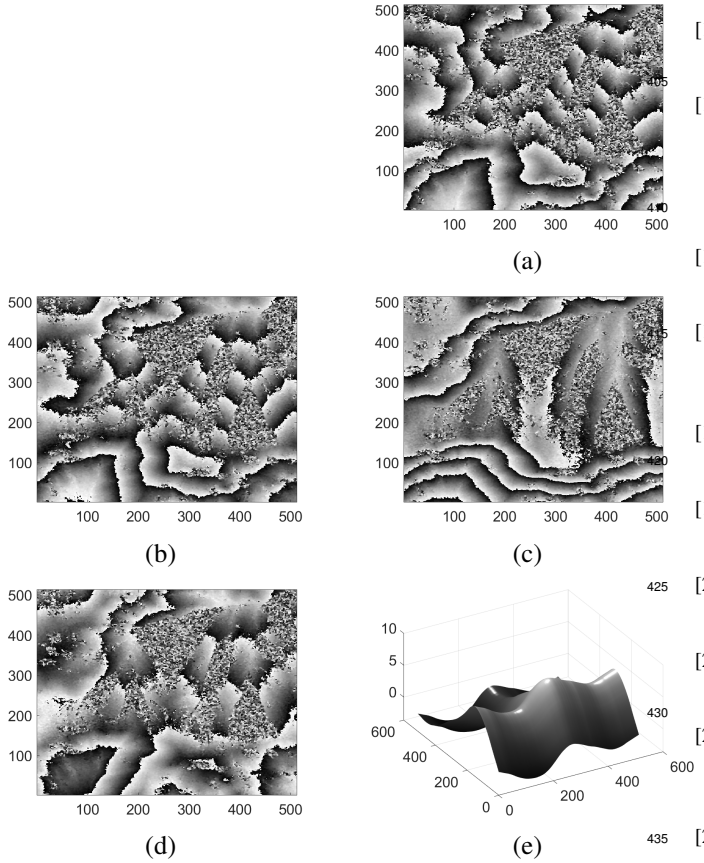

Figure 13: Comparative analysis of algorithms in a wrapped signal that corresponds to the measurement of the upper body mannequin. (a) original wrapped signal obtained by the FFT method [3], including an integer phase shift in the frequency domain; remaining signal component signal after (b) application of carrier removal by the the average slope method [25]; (c) alternative FFT-based wrap reduction method presented in [31]; and (d) the proposed approach. The difference between the signals subtracted in (b) and (d) is illustrated in (e).

[7] K. Perry, J. McKelvie, A comparison of phase shifting and fourier methods in the analysis of discontinuous fringe patterns, Optics and Lasers in Engineering 19 (4) (1993) 269–284. doi:https://doi.org/10.1016/0143-8166(93)90068-V.

[8] L. Yan, H. Zhang, R. Zhang, X. Xie, B. Chen, A robust phase unwrapping algorithm based on reliability mask and weighted minimum least-squares method, Optics and Lasers in Engineering 112 (2019) 39–45. doi:https://doi.org/10.1016/j.optlaseng.2018.08.024.

[9] Z. Zhao, H. Zhao, L. Zhang, F. Gao, Y. Qin, H. Du, 2D phase unwrapping algorithm for interferometric applications based on derivative Zernike polynomial fitting technique, Measurement Science and Technology 26 (1) (2015) 017001.

[10] M. Rivera, F. J. Hernandez-Lopez, A. Gonzalez, Phase unwrapping by accumulation of residual maps, Optics and Lasers in Engineering 64 (2015) 51 – 58. doi:http://dx.doi.org/10.1016/j.optlaseng.2014.07.005.

[11] Q. Huang, H. Zhou, S. Dong, S. Xu, Parallel branch-cut algorithm based on simulated annealing for large-scale phase unwrapping, IEEE Transactions on Geoscience and Remote Sensing 53 (7) (2015) 3833–3846. doi:10.1109/TGRS.2014.2385482.

[12] J. Xu, D. An, X. Huang, P. Yi, An efficient minimum-discontinuity phase-unwrapping method, IEEE Geoscience and Remote Sensing Letters 13 (5) (2016) 666–670.

[13] M. A. Herráez, D. R. Burton, M. J. Lalor, M. A. Gdeisat, Fast two-dimensional phase-unwrapping algorithm based on sorting by reliability following a noncontinuous path, Appl. Opt. 41 (35) (2002) 7437–7444.

[14] H. Zhong, J. Tang, S. Zhang, Phase quality map based on local multi-unwrapped results for two-dimensional phase unwrapping, Applied Optics 54 (4) (2015) 739–745. doi:10.1364/AO.54.000739.

[15] C. Ojha, M. Manunta, A. Pepe, L. Paglia, R. Lanari, An innovative region growing algorithm based on minimum cost flow approach for phase unwrapping of full-resolution differential interferograms, in: IEEE International Conference on Geoscience and Remote Sensing Symposium (IGARSS), 2012, pp. 5582–5585. doi:10.1109/IGARSS.2012.6352054.

[16] M. A. Herráez, J. G. Boticario, M. J. Lalor, D. R. Burton, Agglomerative clustering-based approach for two-dimensional phase unwrapping, Appl. Opt. 44 (7) (2005) 1129–1140.

[17] T. Zhang, S. Jiang, Z. Zhao, K. Dixit, X. Zhou, J. Hou, Y. Zhang, C. Yan, Rapid and robust two-dimensional phase unwrapping via deep learning, Opt. Express 27 (16) (2019) 23173–23185. doi:10.1364/OE.27.023173.

[18] J. Qian, S. Feng, T. Tao, Y. Hu, Y. Li, Q. Chen, C. Zuo, Deep-learning-enabled geometric constraints and phase unwrapping for single-shot absolute 3d shape measurement, Apl Photonics 5 (4) (2020) 046105.

[19] T. Bentahar, A. Bentahar, R. Saidi, H. Mayache, K. Ferroudji, Hybrid technique of the branch-cut and the quality-guided for insar phase unwrapping, International Journal of Image and Graphics (2021) 2150040.

[20] L. Zhou, H. Yu, Y. Lan, M. Xing, Deep learning-based branch-cut method for insar two-dimensional phase unwrapping, IEEE Transactions on Geoscience and Remote Sensing.

[21] M. Takeda, K. Mutoh, Fourier transform profilometry for the automatic measurement of 3-d object shapes, Appl. Opt. 22 (24) (1983) 3977–3982. doi:10.1364/AO.22.003977.

[22] B. Lan, G. Feng, T. Zhang, S. Zhou, Accurate carrier-removal method for interferogram analysis, Optical Engineering 56 (3) (2017) 034101, publisher: International Society for Optics and Photonics. doi:10.1117/1.OE.56.3.034101.

[23] Z. Zhang, F. Wang, G. Xu, J. Jia, X. Liu, Y. Cao, Improved Carrier Frequency-Shifting Algorithm Based on 2-FFT for Phase Wrap Reduction, Mathematical Problems in EngineeringPublisher: Hindawi Limited. doi:10.1155/2021/6664841.

[24] A spatial algorithm to reduce phase wraps from two dimensional signals in fringe projection profilometry 82. doi:10.1016/j.optlaseng.2015.11.009.

[25] J.-L. Li, X.-Y. Su, H.-J. Su, S. S. Cha, Removal of carrier frequency in phase-shifting techniques, Optics and Lasers in Engineering 30 (1) (1998) 107–115. doi:10.1016/S0143-8166(97)00061-4.

[26] Q. Zhang, Z. Wu, A carrier removal method in fourier transform profilometry with zernike polynomials, Optics and Lasers in Engineering 51 (3) (2013) 253–260. doi:https://doi.org/10.1016/j.optlaseng.2012.10.004.

[27] H.-Y. Su, J.-L. Li, X. Su, Phase algorithm without the influence of carrier frequency, Optical Engineering 36 (6) (1997) 1799 – 1805. doi:10.1117/1.601324.

[28] M. Qudeisat, M. Gdeisat, D. Burton, F. Lilley, A simple method for phase wraps elimination or reduction in spatial fringe patterns, Optics Communications 284 (21) (2011) 5105 – 5109.

[29] M. Gdeisat, Performance evaluation and acceleration of flynn phase unwrapping algorithm using wraps reduction algorithms, Optics and Lasers in Engineering 110 (2018) 172–178. doi:https://doi.org/10.1016/j.optlaseng.2018.02.014.

[30] M. Wang, G. Du, C. Zhou, S. Si, Z. Lei, X. Li, Y. Li, Precise and fast phase wraps reduction in fringe projection profilometry, Journal of Modern Optics 64 (18) (2017) 1862–1869. doi:10.1080/09500340.2017.1322719.

[31] M. Arevalillo-Herráez, M. Cobos, M. García-Pineda, A Robust Wrap Reduction Algorithm for Fringe Projection Profilometry and Applications in Magnetic Resonance Imaging, IEEE Transactions on Image Processing 26 (3) (2017) 1452–1465, conference Name: IEEE Transactions on Image Processing. doi:10.1109/TIP.2017.2651378.

[32] D. R. Burton, A. J. Goodall, J. T. Atkinson, M. J. Lalor, The use of carrier frequency shifting for the elimination of phase discontinuities in Fourier transform profilometry, Optics and Lasers in Engineering 23 (4) (1995) 245–257. doi:10.1016/0143-8166(95)00005-9.

[33] Y. Du, G. Feng, H. Li, S. Zhou, Accurate carrier-removal technique based

on zero padding in Fourier transform method for carrier interferogram analysis, Optik 125 (3) (2014) 1056–1061. doi:10.1016/j.ijleo.2013.07.145.

[34] L. Chen, C. J. Tay, Carrier phase component removal: a generalized least-squares approach, J. Opt. Soc. Am. A 23 (2) (2006) 435–443. doi:10.1364/JOSAA.23.000435.

[35] H. C. So, F. K. W. Chan, W. H. Lau, C.-F. Chan, An Efficient Approach for Two-Dimensional Parameter Estimation of a Single-Tone, IEEE Transactions on Signal Processing 58 (4) (2010) 1999–2009, conference Name: IEEE Transactions on Signal Processing. doi:10.1109/TSP.2009.2038962.